NJC

Accepted Manuscript

This is an *Accepted Manuscript*, which has been through the Royal Society of Chemistry peer review process and has been accepted for publication.

Accepted Manuscripts are published online shortly after acceptance, before technical editing, formatting and proof reading. Using this free service, authors can make their results available to the community, in citable form, before we publish the edited article. We will replace this *Accepted Manuscript* with the edited and formatted *Advance Article* as soon as it is available.

You can find more information about *Accepted Manuscripts* in the Information for Authors.

Please note that technical editing may introduce minor changes to the text and/or graphics, which may alter content. The journal's standard Terms & Conditions and the Ethical guidelines still apply. In no event shall the Royal Society of Chemistry be held responsible for any errors or omissions in this *Accepted Manuscript* or any consequences arising from the use of any information it contains.

ROYAL SOCIETY OF CHEMISTRY

www.rsc.org/njc

New Journal of Chemistry Dynamic Article Links ►

Cite this: DOI: 10.1039/c0xx00000x

www.rsc.org/xxxxxx

Full paper

In situ growth of Au nanoparticles on 3D $Bi_2O_2CO_3$ for surface plasmon enhanced visible light photocatalysis

Rui Wang,[a] Xinwei Li,[a] Wen Cui,[a] Yuxin Zhang,[b,*] and Fan Dong [a,c,*]

Abstract: Novel plasmonic photocatalysts were fabricated by the modification of 3D $Bi_2O_2CO_3$ microspheres with Au nanoparticles (NPs) via a facile one-pot in situ method for the first time. The as-obtained 3D Au/$Bi_2O_2CO_3$ heterostructures (Au/BOC) were characterized by XRD, XPS, SEM, TEM, EDX, N_2 adsorption–desorption isotherms, UV–vis DRS and PL. The results revealed that the Au NPs were produced from in situ reduction of Au^{3+} by the citrate ions and deposited on the surface of $Bi_2O_2CO_3$ microspheres. The photocatalytic activity of Au/BOC was evaluated by removal of NO under visible light with the pure $Bi_2O_2CO_3$ as reference. The pure $Bi_2O_2CO_3$ microspheres displayed decent photocatalytic activity due to the surface scattering and reflecting (SSR) resulted from the special hierarchical architecture. The Au/BOC exhibited highly enhanced visible light photocatalytic performance in comparison with the pure BOC because of the co-contribution of the SSR effect, the Schottky barrier and the surface plasmon resonance (SPR) effect endowed with metallic Au NPs. The integration of the SSR effect and SPR effect on one system for enhancing photocatalysis could provide a new scope in architecture design and mechanism understanding of other noble metal-based plasmonic photocatalysts.

1. Introduction

Environment pollution and energy shortage remain to be the two global challenges that influence the sustainable development of human beings. As a green technology, semiconductor photocatalysis is expected to become one of the most effective ways to solve these challenges. With photocatalysis, solar light/visible light can be potentially utilized to achieve efficient pollutants degradation, solar energy conversion and organic synthesis.[1-7]

Since Fujishima et al. carried out the research of TiO_2 photoelectrode water splitting in 1972, TiO_2 has been by far the most studied photocatalyst.[8] In recent years, except for diverse modification of TiO_2 for extending visible light absorption, such as doping with metals and nonmetals, sensitizing with dyes, compositing with matched semiconductor and forming heterojunction with noble metals,[5,9,10] other kinds of non-TiO_2 based visible light photocatalytic materials have also been developed rapidly. These new photocatalysts include bismuth-based semiconductors, polymer-based semiconductors (e.g. g-C_3N_4), and metal-based elements (Au, Ag, Bi).[11-14] Among them, $Bi_2O_2CO_3$, as one of the emergent bismuth-based semiconductors, has received increased attention for its broad applications in antibacterial, environmental remediation, and super capacitor.[15-20] For instance, Cheng et al. prepared hierarchical $Bi_2O_2CO_3$ composed of 2D nanosheets which showed enhanced photocatalytic degradation of organic dyes.[21] Chen and co-workers have synthesized $Bi_2O_2CO_3$ nanotubes through a refluxed solvothermal method with admirable antibacterial properties against Helicobacter pylori.[22] However, the large band gap of pure $Bi_2O_2CO_3$ (3.1 to 3.5 eV) makes it unable to utilize the abundant visible light. Much effort has been devoted to the improvement of visible light photocatalytic performance of $Bi_2O_2CO_3$ via various modification methods. Yu et al. constructed hierarchical graphene-$Bi_2O_2CO_3$ composites which exhibit significantly enhanced visible light

[a] Chongqing Key Laboratory of Catalysis and Functional Organic Molecules, College of Environment and Resources, Chongqing Technology and Business University, Chongqing, 400067, China.
[b] College of Materials Science and Engineering, National Key Laboratory of Fundamental Science of Micro/Nano-Devices and System Technology, Chongqing University, Chongqing, 400044, China.
[c] Engineering Research Center for Waste Oil Recovery Technology and Equipment, Ministry of Education, Chongqing Technology and Business University, Chongqing, 400067, China.
*To whom correspondence should be addressed.
E-mail: dfctbu@126.com (Fan Dong). zhangyuxin@cqu.edu.cn (Yuxin Zhang), Tel.: +86-23-62769785-605; Fax: +86-23-62769785-605.

photocatalytic performance.[23] Novel Ag/$Bi_2O_2CO_3$ composites were fabricated by Peng's group, exhibiting outstanding photocatalytic and supercapacitive properties.[24] Our group has exploited a template-free method for fabrication of N-doped $Bi_2O_2CO_3$ hierarchical microspheres.[25-27] And subsequently, we have achieved controlling the crystal and morphological structure of N-doped $Bi_2O_2CO_3$ including rose-like, hydrangea flower-like and peony flower-like microspheres by tuning the hydrothermal temperature.

Recently, the utilization of surface plasmon resonance (SPR) of noble metal nanoparticles (Ag or Au) to improve the activity of semiconductor photocatalysts has been widely investigated.[28-30] The mechanism of SPR effect that enhances the catalytic activity and efficiency is known to act in three aspects[31]: (i) the increased scattering effect of resonant photon, (ii) the hot electron-holes produced in metal, (iii) the plasmonic energy transfer from metal to the semicondutor via the created electric field enhancement of localized plasmons. The plasmon resonance energy transfer of the SPR phenomena can enhance the electric field created around the metal where the energy can transfer from the noble metal NPs to the adjacent semiconductor, and promote the formation of electrons/holes, finally enhancing photocatalytic activity under visible light.[32-35] What is more, the combination of plasmonic particles with semconductor photocatalysts has been reported for various chemical reactions, such as oxidation reactions of organic molecules (gas phase), and water splitting (liquid phase).[36,37] For example, TiO_2, CeO_2 and ZnO combined with the plasmonic Au particles showed greatly promoted photocatalytic activity under visible light irradiation as a result of the strong surface plasmon resonance excitation of such noble metals.[38,39] Very recently, Au nanoparticles has been deposited on $Bi_2O_2CO_3$ microspheres to improve photocatalysis via a multi-step method.[40] To seek simple-but-effective preparation method and reduce production cost, it is highly desirable to develop a one-step method for the fabrication of Au/$Bi_2O_2CO_3$ microspheres.

Here, a facile one-pot in situ method for synthesis of 3D Au/$Bi_2O_2CO_3$ heterostructures was developed. The Au^{3+} from the $HAuCl_4$ precursor was in situ reduced to metallic Au particles by citrate ions from bismuth citrate. The Au nanoparticles are thereby in situ loaded on the surface of $Bi_2O_2CO_3$ microspheres, making the as-obtained 3D Au/$Bi_2O_2CO_3$ heterostructures highly visible light active. In our previous work, we have demonstrated that the special 3D hierarchical structure could make the pure $Bi_2O_2CO_3$ visible light active due to its surface scattering and reflecting effect (SSR effect).[41] In the present work, we found that the Au/$Bi_2O_2CO_3$ heterostructures exhibited highly enhanced visible light photocatalytic activity. On the one hand, the enhanced visible light activity of the Au/$Bi_2O_2CO_3$ can be ascribed to the accelerated the electron/hole separation through a Schottky barrier at the interface.[28,42,43] On the other hand, the energy can transfer from the Au NPs to the $Bi_2O_2CO_3$ via the electric field created around the Au NPs resulted in the increased formation of electrons/holes.[34] With the cooperation of the SSR effect, Schottky barrier and SPR effect, a highly efficient visible light photocatalyst can be developed, which could provide some new insights in architecture design and synthesis of other photocatalysts.

2. Experimental

2.1 Materials and synthesis

All the reagents used in this research were of analytical grade and used as received without further purification. In a typical synthesis, 0.46 g of sodium carbonate was added into a 100 mL autoclave Teflon vessel with 70 ml H_2O and stirred for 10 min. Then, appropriate amount of $HAuCl_4$ (0.342g) solution was dissolved in 100 mL H_2O for further use. The $HAuCl_4$ solution (10 mL) was added into aqueous sodium carbonate and stirred for 10 min. After that, bismuth citrate (1.60 g) was added and stirred for another 30 min. The resulting precursor suspension was then hydrothermally treated at 160 ^oC for 24 h. The Au/$Bi_2O_2CO_3$ hierarchical microspheres (Au-BOC) was filtered, washed with water and ethanol three times and dried at 70 ^oC to get final Au/$Bi_2O_2CO_3$ hierarchical microspheres (Au-BOC) without any further treatment. The mole fraction of Au in the composite was 5.0 %.

2.2. Characterization

X-ray diffraction was taken to analyze the crystal phases of the sample with Cu Kα radiation (XRD: model D/max RA, Rigaku Co., Japan). FT-IR spectra were obtained using a Nicolet Nexus spectrometer on samples embedded in KBr pellets. X-ray photoelectron spectroscopy was used with Al Kα X-rays (hv=1486.6 eV) radiation under 150W (XPS: Thermo ESCALAB 250, USA) to inquiry the surface properties and total density of the state (DOS) distribution in the valence band (VB). For characterizing the morphology of the products, SEM images and EDS (SEM, JEOL model JSM-6490, Japan) were used. TEM image was measured to reveal the morphology and structure of the obtained products (TEM: JEM-2010, Japan). The UV–vis diffuse reflection spectra were obtained for the dry-pressed disk samples using a Scan UV–vis spectrophotometer (UV-vis DRS, UV-2450, Shimadzu, Japan) equipped with an integrating sphere assembly, using 100% $BaSO_4$ as reflectance sample. The nitrogen adsorption–desorption isotherm and Barrett–Joyner–Halenda (BJH) methods were finished on a nitrogen adsorption apparatus (ASAP 2020, USA). The Photoluminescence (PL: F-7000, HITACHI, Japan) was used to investigate the charge transfer properties.

2.3. Evaluation of photocatalytic activity

The photocatalytic activity was investigated by removal of NO at ppb levels in a continuous flow reactor at ambient temperature. The volume of the rectangular reactor, made of stainless steel and covered with Saint-Glass, was 4.5 L (30 × 15 × 10 cm). A 100 W commercial tungsten halogen lamp was vertically placed outside the reactor. UV cutoff filter (420 nm) was adopted to remove UV light in the light beam. Photocatalyst (0.10 g) was coated onto a dish with a diameter of 12.0 cm. The coated dish was then pretreated at 70 ^{o}C to remove water in the suspension. For each test, two coated were used. The NO gas was acquired from a compressed gas cylinder at a concentration of 100 ppm of NO (N_2 balance). The initial concentration of NO was diluted to about 600 ppb by the air stream. The desired relative humidity (RH) level of the NO flow was controlled at 50 % by passing the zero air streams through a humidification chamber. The gas streams were premixed completely by a gas blender, and the flow rate was controlled at 2.4 L/min by a mass flow controller. After the adsorption–desorption equilibrium was achieved, the lamp was turned on. The concentration of NO was continuously measured by a chemiluminescence NO analyzer (Thermo Scientific, model 42i-TL), which monitors NO, NO_2, and NO_x (NO_x represents NO + NO_2) with a sampling rate of 1.0 L/min. The NO removal ratio (η) was calculated as η (%) = $(1-C/C_0) \times 100\%$, where C and C_0 are concentrations of NO in the outlet steam and the feeding stream, respectively.

3. Results and discussion

The 3D Au-decorated $Bi_2O_2CO_3$ heterostructures were synthesized by a facile one-pot in situ hydrothermal method and were applied in visible light photocatalytic removal of NO in air.

3.1 Phase structure

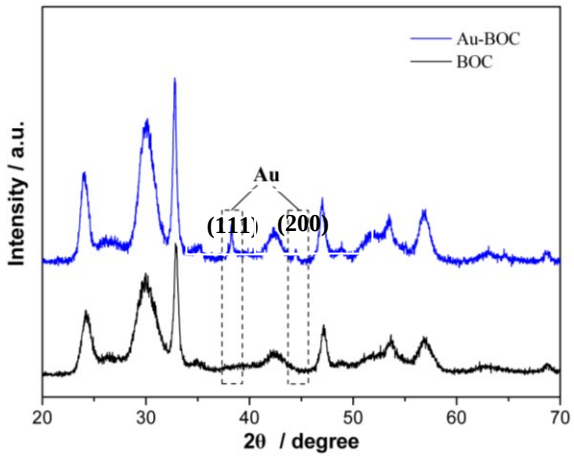

Fig. 1 XRD patterns of BOC and Au-BOC.

The XRD patterns of the as-obtained Au/$Bi_2O_2CO_3$ heterostructures and pure $Bi_2O_2CO_3$ are shown in Fig. 1. The diffraction peaks of pure $Bi_2O_2CO_3$ can be indexed to the standard card of $Bi_2O_2CO_3$ (JCPDS-ICDD Card No. 25-1464). After loading with 5.0 % of Au nanoparticles (Au NPs) on BOC, the typical diffraction peaks of Au (111) and Au (200) can be observed, which indicates the formation of metallic Au. Except for diffraction peaks of Au, the other peaks in Au-BOC could well-match $Bi_2O_2CO_3$ with no impurity peaks, which implies that the presence of Au NPs have no significant influence on the crystal phase of $Bi_2O_2CO_3$. In line with the crystal structure of $Bi_2O_2CO_3$, the $(Bi_2O_2)^{2+}$ layers and CO_3^{2-} layers are orthogonal and inter-grown with the plane of the CO_2^{3-} group. The crystal growth would be preferable to form 2D nanoplate morphology along certain axis under the guidance of this internal layered structure.[44]

3.2. Chemical composition by XPS

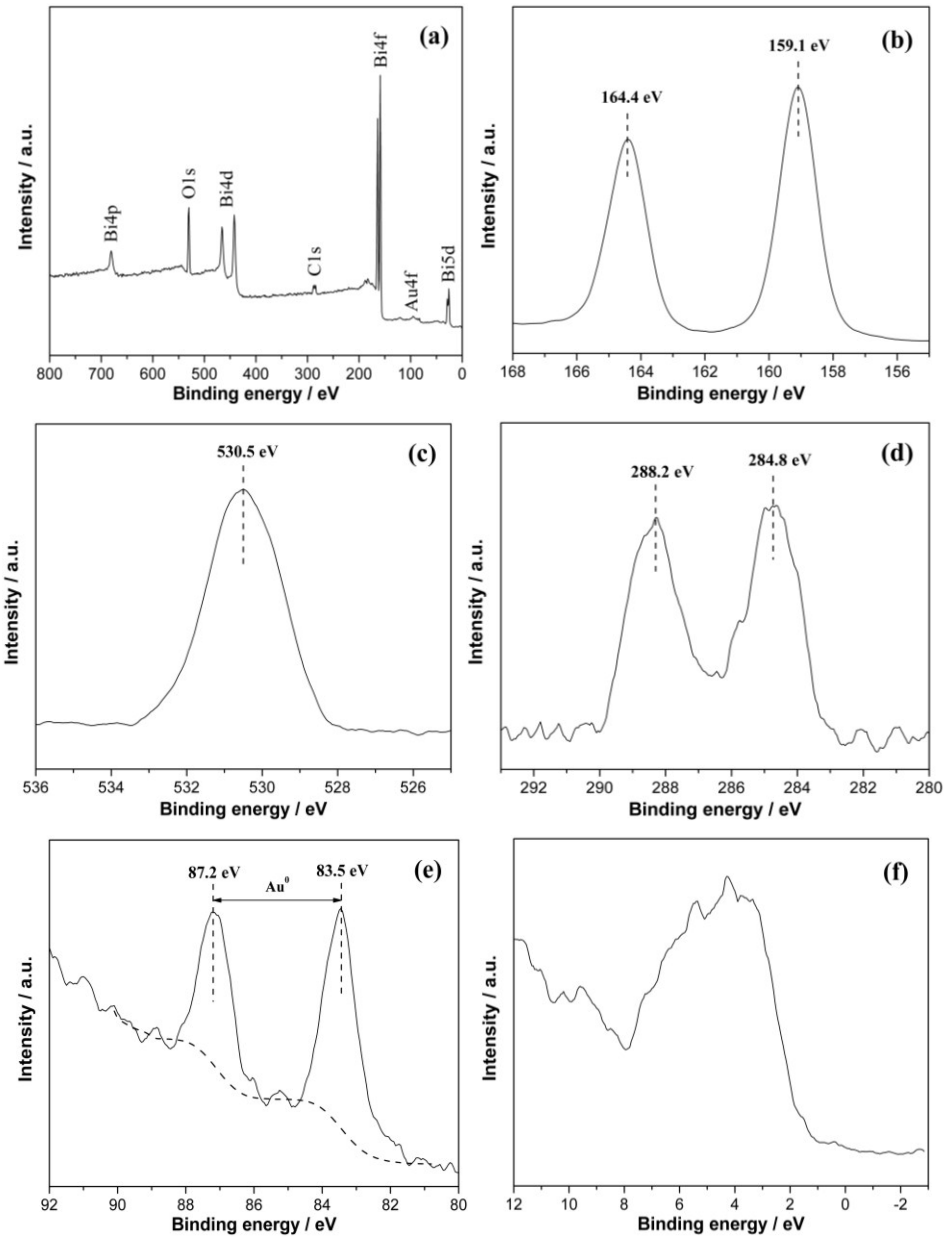

Fig. 2 XPS spectra of Au-BOC, survey (a), Bi 4f (b), O1s (c), C1s (d), Au 4f (e) and valence band (f).

To further confirm the chemical composition of the as-synthesized Au-BOC products, we have carried out X-ray photoelectron spectroscopy (XPS) as shown in Fig. 2. The XPS survey spectra in Fig. 2a show that Bi, O, C and Au elements are included in Au-BOC samples. In Fig. 2b, two strong peaks existing at 159.1 eV and 164.4 eV which emanated from Bi^{3+} in $Bi_2O_2CO_3$ can be allocated for $Bi4f_{7/2}$ and $Bi4f_{5/2}$, respectively.[45] Fig. 2c displays the spectrum of O1s which located at 530.5eV, and this peak can be assigned to the carbonate specials and adsorbed H_2O on the surface of the catalyst.[25] The C1s spectra are recorded as displayed in Fig. 2d, which can be fitted by two peaks at binding energies of 284.8eV and 288.2eV, respectively. The peak at 284.8eV comes from the adventitious carbon from XPS measurement, while the peak at 288.2eV is the characteristic of CO_3^{2-} in $Bi_2O_2CO_3$.[25] Moreover, as presented in Fig. 2e, a binding energy ranging from 88.0 to 82.0 eV can be found for Au 4f. The one at 87.2 eV is corresponding to Au $4f_{5/2}$, while the other one at 83.5 eV belongs to Au $4f_{7/2}$. The binding energy of Au 4f is assigned to metallic Au (0), which indicates that Au^{3+} was reduced to metallic Au by citrate ions. Meanwhile, Fig. 3f shows the DOS of VB for the sample. Notably, the additional electronic states above the VBM can be observed, which originates from the coupled metallic Au.

3.3. Morphological structure

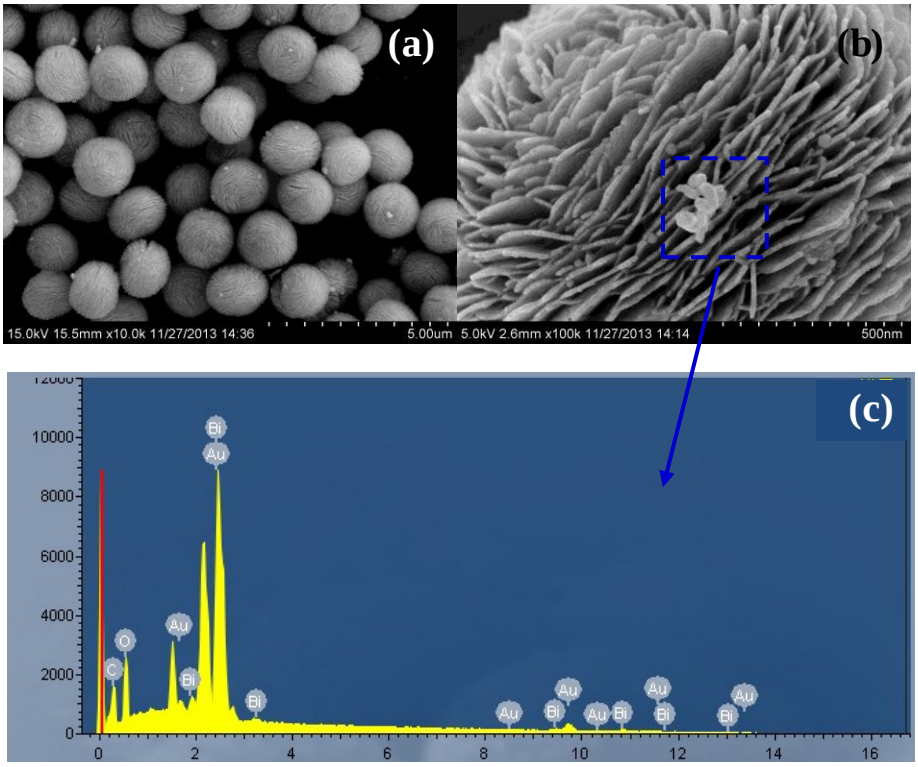

Fig. 3 SEM images of Au-BOC (a, b), and EDX of selected area (c) in (b).

The SEM and TEM were further used to investigate the morphology and microstructure of the as-prepared Au decorated $Bi_2O_2CO_3$ composites. It can be seen in Fig. 3a that many 3D flower-like hierarchical microspheres with a uniform size (diameter ranging from 1.0 to 1.2 μm) can be observed. These microspheres are composed of 2D self-assembled nanosheets. Also, some white particles can be found on the surface of the $Bi_2O_2CO_3$ hierarchical microspheres, which can be assigned to the Au nanoparticles (NPs). This result is well matched with XRD analysis. Fig. 3b shows an amplified area of Au NPs decorated $Bi_2O_2CO_3$ hierarchical microsphere. The corresponding EDX spectra of the selected area in Fig. 3b are displayed in Fig. 3c. The EDX spectra demonstrate that the Au NPs were deposited on the surface of $Bi_2O_2CO_3$ microspheres.

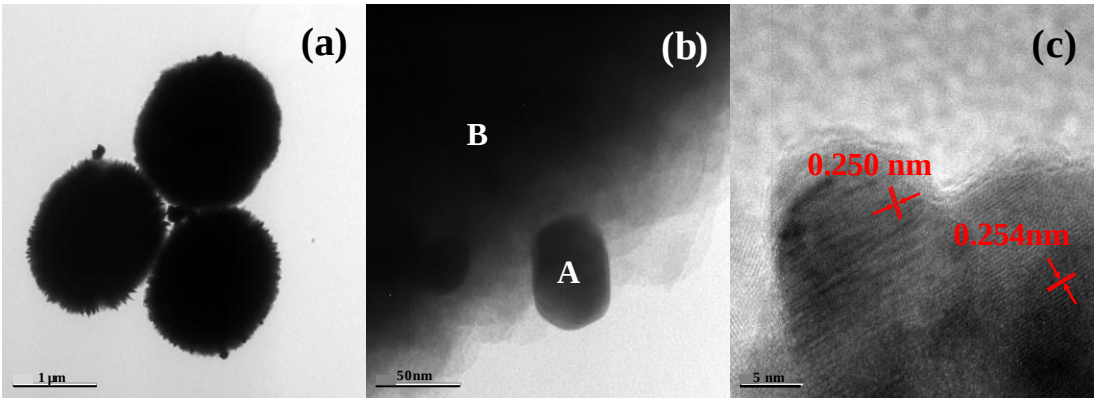

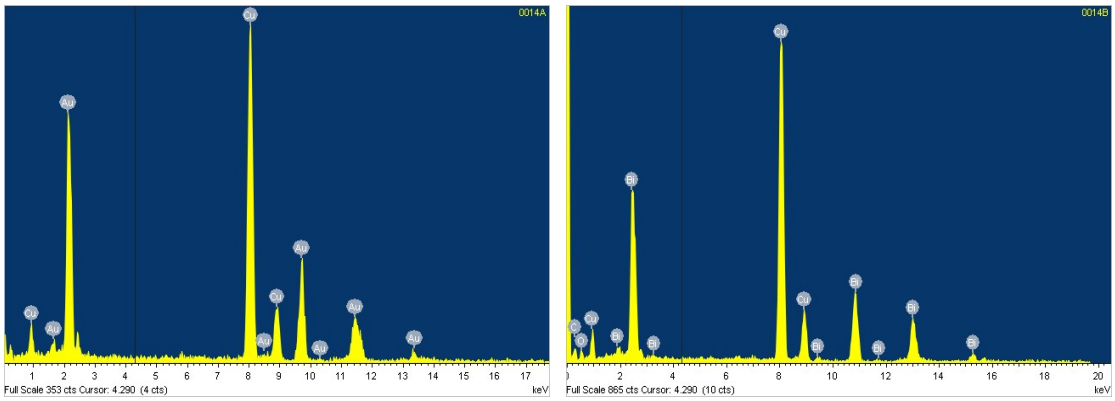

Fig. 4 TEM images of Au-BOC (a, b), HRTEM image (c) and EDX (d, e) of selected area in (b), (d) stands for A area in (b) and (e) stands for B area in (b).

The TEM and HRTEM images of Au-BOC were shown in Fig. 4. From the TEM images in Fig. 4a and 4b of Au-BOC show that microspheres were formed by self-assembled nanosheets with some particles attached on the surface. A typical HRTEM is presented in Fig. 4c. The Au NPs as well as the $Bi_2O_2CO_3$ are all highly crystallized. The lattice spacing of 0.250nm and 0.254 nm are corresponding to Au (111) and tetragonal $Bi_2O_2CO_3$ (112), respectively. Further observation on Fig. 4c indicates that Au NPs are firmly on the surface of $Bi_2O_2CO_3$. The EDX spectra of the selected area A and B in Fig. 4b are presented in Fig. 4d and 4e. In area A, the signal of Au can be clearly detected. In area B, there was no Au signal except for the peaks of Bi, C, and O from $Bi_2O_2CO_3$. These results imply that the Au NPs are deposited on the surface of $Bi_2O_2CO_3$ without doping into the microspheres.

3.4. BET surface areas and pore structure

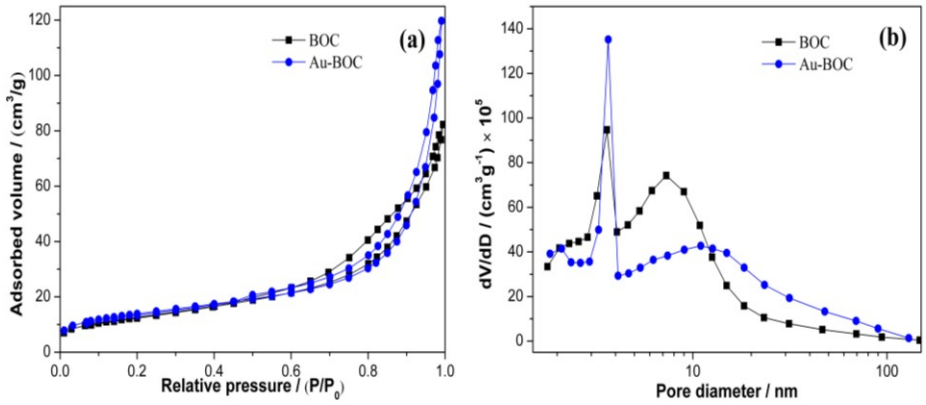

Fig. 5 N_2 adsorption-desorption isotherms (a) and the corresponding pore size distribution curves (b) of BOC and Au-BOC.

The N_2 adsorption–desorption isotherms and corresponding pore size distribution (PSD) curves of the pure BOC and Au-BOC samples are shown in Fig. 5. Both pure BOC and Au-BOC exhibit the representative isotherms of type IV and hysteresis loops type H3 at high relative pressure (P/P_0) between 0.6 and 1.0. These results indicate the presence of mesopores and the formed slit-like pores due to the aggregated sheet-like particles,[46] in compliance with the self-assembled nanosheet-like morphology of Au-BOC samples (Fig. 2 and 3). The corresponding PSD curves are shown in Fig. 5b. The pore distribution of pure BOC and Au-BOC ranged widely from 2.0 to 100 nm. The smaller peak mesopores (~3.6-3.7 nm) can be attributed to the porosity within microspheres. The large peak mesopores (~7.3-10.0 nm) originated from the porous space resulting from the stacked microspheres. As can be seen in Table 1, specific surface areas (S_{BET}), pore volume and pore diameter of the pure BOC and Au-BOC are similar, revealing that the Au NPs were mostly stored on the outer surface of $Bi_2O_2CO_3$ hierarchical microspheres rather than inside the mesoporous channels. This result is also consistent with SEM and TEM observations.

Table 1 The surface areas, pore parameters, band gap, Abs. at 500 nm and NO removal ratio of BOC and Pd-BOC.

Samples	S_{BET}	Total volume	Peak diameter	Band gap	Abs at 500	NO removal ratio

	(m^2/g)	(cm^3/g)	(nm)	(eV)	nm	(%)
BOC	46	0.177	3.6/7.3	3.40	0	23.4
Au-BOC	49	0.185	3.7/11.0	3.40	0.125	56.4

3.5 UV-vis DRS and PL

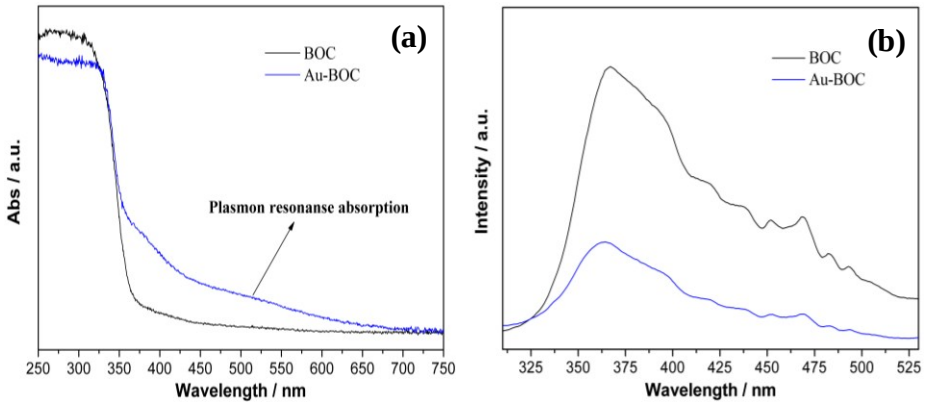

Fig. 6 UV-vis DRS (a) and PL (b) of BOC and Au-BOC.

For better elucidation of the effect of Au deposition on photocatalytic activity of $Bi_2O_2CO_3$, the closely related optical properties of Au/$Bi_2O_2CO_3$ composites as well as that of the pure $Bi_2O_2CO_3$ reference are examined by the UV-vis DRS as shown in Fig. 6a. The pure $Bi_2O_2CO_3$ hierarchical microspheres displays weak response in visible light, which is associated with reflecting and scattering effect resulting from the special 3D hierarchical structure.[41] The Au-BOC exhibits higher absorption in the visible light region from 450 to 600 nm than that of pure $Bi_2O_2CO_3$ microspheres, which is directly ascribed to the surface plasmon resonance absorption of Au NPs that enhances the visible light absorption.[47-49]

The PL measurement could provide important information on charge separation. As can be seen in Fig. 6b that the PL intensity of Au-BOC is much lower than that of pure BOC, which implies that Au/$Bi_2O_2CO_3$ heterostructures can significantly restrain the recombination of electron–hole pairs with the role of Au NPs as electron traps to promote electron–hole separation via creating a Schottky barrier at the interface.[28,43, 50] Once Au NPs are coupled on $Bi_2O_2CO_3$ microspheres to form Au/$Bi_2O_2CO_3$ heterostructures, the speed of charge separation at the Au/$Bi_2O_2CO_3$ interface can be expedited accordingly and the photo-excited electrons could transfer from the CB of $Bi_2O_2CO_3$ to the Au NPs, thus inhibiting the e–h pair recombination.[28,51]

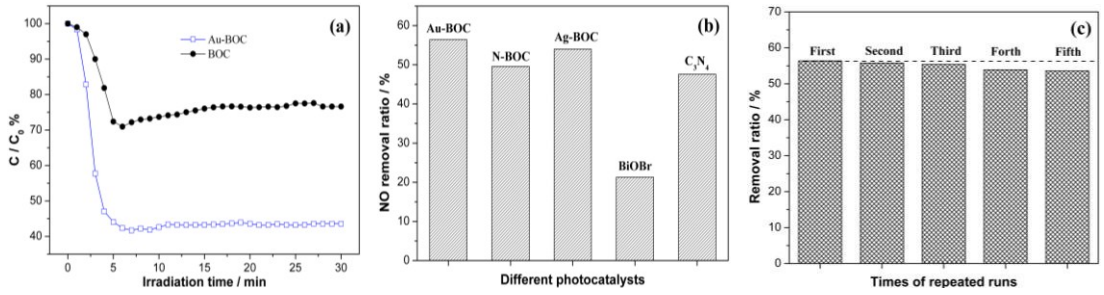

Fig. 7 Visible light photocatalytic activity of BOC and Au-BOC (a) in comparison with the activity of different photocatalyst under the same conditions (b) for NO removal and the repeated visible light photocatalytic activity of Au-BOC (c).

The photocatalytic property of the as-obtained samples is performed under visible light irradiation by removal of NO in air to prove their potential ability in air purification. The variation of NO concentration (C/C_0 %) under visible light irradiation with irradiation time over BOC and Au-BOC are presented in Fig. 7a. Previous reports showed that no obvious decrease in NO concentration were observed without light irradiation or photocatalyst.

With the presence of visible light and photocatalyst, NO could react with the photo-generated reactive radicals and subsequently create final product of HNO_2 and HNO_3.[52,53]

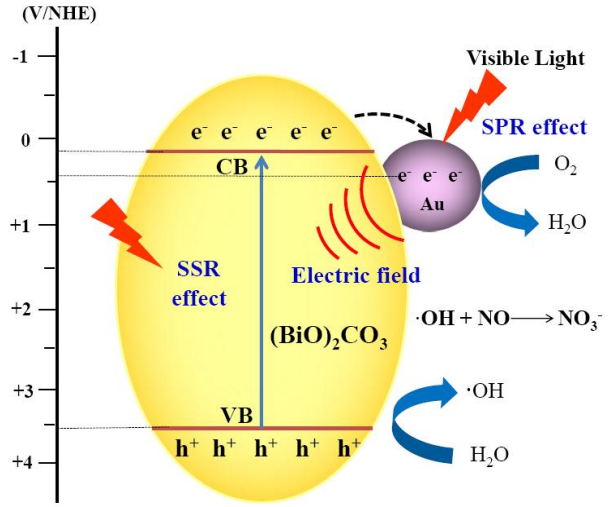

Fig. 8 Photocatalytic mechanism scheme of Au-decorated $Bi_2O_2CO_3$ under visible light irradiation.

In Fig. 7a, it can be seen that both pure BOC and Au-BOC are able to photocatalyze the oxidation of NO in air under visible light irradiation while the NO removal ratio of pure BOC (23.4%) is allocated for its special hierarchical microspheres structure that enables the multiple light surface scattering and reflecting effect which improves the effective optical path-length of a photon as well as absorption probability.[54] Previous report on BiOCl hierarchical nanostructures demonstrated similar phenomenon.[54] For Au decorated $Bi_2O_2CO_3$, the samples display prominent photocatalytic property with the NO removal ration of 56.4%, higher than that of N-doped $Bi_2O_2CO_3$ (49.6%),[55] Ag-decorated $Bi_2O_2CO_3$ (54.0%),[56] BiOBr (21.3%),[57] and C_3N_4/C_3N_4 heterostructures (47.6 %) under similar test conditions.[58] The repeated runs of NO photocatalytic removal under visible light was carried out to investigate the photocatalytic stability of the Au -decorated $Bi_2O_2CO_3$. As can be seen in Fig. 7c, the Au-BOC sample remains to be durable in repeated photocatalytic runs with no distinct deactivation. This results indicates that the obtained Au/ $Bi_2O_2CO_3$ catalyst is stable under irradiation. The highly enhanced photocatalytic performance of Au-BOC can be ascribed to the plasmon induced electric field created around Au (as shown in Fig. 8) which promotes the formation rate of electron-holes,[32-35] and the Schottky barrier that could enhance the interfacial electron transfer.[42,59,60]

Beyond that, as can be seen in Fig. 8, the electrons from CB of $Bi_2O_2CO_3$ under the visible light irradiation could transfer onto Au NPs as the Fermi level of metallic Au (0.45 eV) is lower than that of the CB of $Bi_2O_2CO_3$ (0.20 eV). As the the Fermi level of Au is more positive than that of the redox potential of $O_2/\cdot O_2^-$ (-0.33 eV), the electrons from Au NPs could reduce O_2 to form H_2O via multiple electron process.[59] At the same time, the holes in the VB of $Bi_2O_2CO_3$ are capable of oxidizing H_2O into ·OH radicals for NO oxidation to final NO_2^- and NO_3^- products.[61]

4. Conclusion

To sum up, a facile one-pot in situ method for synthesis of three dimensional Au/$Bi_2O_2CO_3$ heterostructures was developed for the first time. The coupled Au nanoparticles were in situ reduced from Au^{3+} by the citrate ions during the hydrothermal process and subsequently deposited on the surface of the $Bi_2O_2CO_3$ microspheres. This Au/$Bi_2O_2CO_3$ heterostructures exhibited highly enhanced photocatalytic activity and stability for the removal of nitric monoxide in air under visible light irradiation. The efficient activity of Au/$Bi_2O_2CO_3$ can be ascribed to the cooperative promotiom effects of the surface scattering and reflecting effect, the Schottky barrier and the surface plasmon resonance effect endowed with metallic Au nanoparticles. These effects combined could enable the Au/$Bi_2O_2CO_3$ composites to be a promising visible light photocatalyst for air purification. The in situ preparation method could also be extended for other plasmonic photocatalysts and provide a new insight on future photocatalysts development.

Acknowledgements

This research was financially supported by the National Natural Science Foundation of China (51478070, 51108487), and the Science and Technology Project from Chongqing Education Commission (KJZH14210).

References

1 S.W. Cao, J.X. Low, J.G. Yu and M. Jaroniec, Adv. Mater., 2015, **27**, 2150–2176.
2 N. Zhang, R. Ciriminna, M. Pagliaro and Y. J. Xu, Chem. Soc. Rev., 2014, **43**, 5276–5287.
3 H.W. Huang, X. Han, X.w. Li, S.C. Wang, P.K. Chu and Y.H. Zhang, ACS Appl. Mater. Interfaces, 2015, **7**, 482–492.
4 J. Li, Y. Yu and L. Z. Zhang, Nanoscale, 2014, **6**, 8473–8488.
5 W.J. Jiang, J.A. Joens, D.D. Dionysiou**,** K.E. O'Shea, J. Photochem. Photobiol. A: Chem. 2013, **262**, 7–13.
6 H.W. Huang, Y. He, Z.H. Lin, L. Kang and Y.H. Zhang, J. Phys. Chem. C, 2013, **117**, 22986−22994.
7 H. F. Cheng, B. B. Huang and Y. Dai, Nanoscale, 2014, **6**, 2009–2026.
8 A. Fujishima and K. Honda, Nature, 1972, **238**, 37–38.
9 G. Liu, L.Z. Wang, H.G. Yang, H.M. Cheng and G.Q. Lu, J. Mater. Chem. 2010, **20**, 831–843.
10 H. Tong, S.X. Ouyang, Y.P. Bi, N. Umezawa, M. Oshikiri and J.H. Ye, Adv. Mater. 2012, **24**, 229–251.
11 L.S. Zhang, W.Z. Wang, L. Zhou and H.L. Xu, Small, 2007, **3**, 1618–1625.
12 Y. Wang, X.C. Wang and M. Antonietti, Angew. Chem. Int. Ed. 2012, **51**, 68–89.
13 V. Subramanian, E.E. Wolf and P.V. Kamat, J. Am. Chem. Soc. 2004, **126**, 4943–4950.
14 Z.K. Zheng, B.B. Huang, X.Y. Qin, X.Y. Zhang, Y. Dai and M.H. Whangbo, J. Mater. Chem. 2011, **21**, 9079–9087.
15 F. Dong, A.M. Zheng, Y.J. Sun, M. Fu, B.Q. Jiang, W.K. Ho, S.C. Lee, and Z.B. Wu, CrystEngComm, 2012, **14**, 3534–3544.
16 F. Dong, J. Bian, Y.J. Sun, T. Xiong and W.D. Zhang, CrystEngComm, 2014, **16**, 3592–3604.
17 Y.Y. Liu, Z.Y. Wang, B.B. Huang, K.S. Yang, X.Y. Zhang, X.Y. Qin and Y. Dai, Appl. Surf. Sci. 2010, **257**, 172–175.
18 Y. Zheng, F. Duan, M.Q. Chen and Y. Xie, J. Mol. Catal. A: Chem. 2010, **317**, 34–40.
19 T. Xiong, H.W. Huang, Y.J. Sun and F. Dong, J. Mater. Chem. A, 2015, 3, 6118–6127.
20 J.J. Ma, S.J. Zhu, Q.Y. Shan, S.F. Liu, Y.X. Zhang, F. Dong and H.D. Liu, Electrochimica Acta, 2015, **168**, 97–103.
21 P. Madhusudan, J. Zhang, B. Cheng and G. Liu, CrystEngComm, 2013, **15**, 231–240.
22 R. Chen, M.H. So, J. Yang, F. Deng, C.M. Che and H.Z. Sun, Chem. Commun. 2006, **42**, 2265–2267.
23 P. Madhusudan, J.G. Yu, W.G. Wang, B. Cheng and G. Liu, Dalton Trans. 2012, **41**, 14345–14353.
24 S.J. Peng, L.L. Li, H.T. Tan, Y.Z. Wu, R. Cai, H. Yu, X. Huang, P.N. Zhu, S. Ramakrishna, M. Srinivasan and Q.Y. Yan, J. Mater. Chem. A, 2013, **1**, 7630–7638.
25 F. Dong, Y.J. Sun, M. Fu, W.K. Ho, S.C. Lee and Z.B. Wu, Langmuir, 2012, **28**, 766−773.
26 F. Dong, Y.J. Sun, W.K. Ho and Z.B. Wu, Dalton Trans. 2012, **41**, 8270−8284.
27 F. Dong, T. Xiong, Z.W. Zhang, Y.J. Sun and M. Fu, CrystEngComm, 2013, **15**, 10522−10532.
28 Z.F. Bian, T. Tachikawa, P. Zhang, M. Fujitsuka and T. Majima, J. Am. Chem. Soc. 2014, **136**, 458−465.
29 S. Sun, H.Z. Liu, L. Wu, C.E. Png and P. Bai, ACS Catal. 2014, **4**, 4269−4276.
30 H.Y. Li, W.B. Lu, J.Q. Tian, Y.L. Luo, A.M. Asiri, A.O. Al-Youbi and X.P. Sun, Chem. Eur. J. 2012, **18**, 8508−8514.
31 D.B. Ingram, P. Christopher, J.L. Bauer and S. Linic, ACS Catal. 2011, **1**, 1441−1447.
32 C.L. Wang and D. Astruc, Chem. Soc. Rev. 2014, **43**, 7188−7216.
33 S.C. Warren and E. Thimsen, Energy & Environmental Science, 2012, **5**, 5133−5146.
34 Y.H. Tseng, I.G. Chang, Y. Tai and K.W. Wu, J. Nanosci. Nanotechnol. 2012, **12**, 416−422.
35 W. Hou, Z. Liu, P. Pavaskar, W.H. Hung and S.B. Cronin, J. Catal. 2011, **277**, 149−153.
36 D. Tsukamoto, Y. Shiraishi, Y. Sugano, S. Ichikawa, S. Tanaka and T. Hirai, J. Am. Chem. Soc. 2012, 134, 6309–6315.
37 J.J. Chen, J.C.S. Wu, P.C. Wu and D.P. Tsai, J. Phys. Chem. C, 2011, **115**, 210−216.
38 S. Naya, A. Inoue and H. Tada, J. Am. Chem. Soc. 2010, **132**, 6292−6293.
39 Z.W. Liu, W.B. Hou, P. Pavaskar, M. Aykol and S.B. Cronin, Nano Lett. 2011, **11**, 1111−1116.
40 Q.Y. Li, X.D. Hao, X.L. Guo, F. Dong and Y.X. Zhang, Dalton Trans. 2015, **44**, 8805−8811.
41 T. Xiong, F. Dong and Z.B. Wu, RSC Adv. 2014, **4**, 56307−56312.
42 M.J. Kale, T. Avanesian and P. Christopher, ACS Catal. 2014, **4**, 116−128.
43 D.Q. Zhang, M.C. Wen, S.S. Zhang, P.J. Liu, W. Zhu, G.S. Li and H.X. Li, Appl. Catal., B: Environ. 2014, **147**, 610–616.
44 C.Z. Wu and Y. Xie, Chem. Commun. 2009, **40**, 5943–5957.
45 S. Shamaila, A.K.L. Sajjad, F. Chen and J.L. Zhang, Appl. Catal. B, 2010, **94**, 272–280.
46 J. Zhang, J.G. Yu, Y.M. Zhang, Q. Li and J.R. Gong, Nano Lett. 2011, **11**, 4774–4779.
47 P. Englebienne, Analyst, 1998, **123**, 1599−1603.
48 J. Prikulis, P. Hanarp, L. Olofsson, D. Sutherl and M. Kaell, Nano Lett, 2004, **4**, 1003−1007.
49 Y. Sun and Y. Xia, Anal. Chem. 2002, **74**, 5297−5305.
50 G. Schubert, A. Gazsi and F. Solymosi, J. Catal. 2014, **313**, 127–134.

51 K. Qian, B.C. Sweeny, A.C. Johnston-Peck, W.X. Niu, J.O. Graham, J.S.D. Chene, J.J. Qiu, Y.C. Wang, M.H. Engelhard, D. Su, E.A. Stach and W.D. Wei, J. Am. Chem. Soc. 2014, **136**, 9842−9845.
52 F. Dong, S.C. Lee, Z.B. Wu, Y. Huang, M. Fu, W.K. Ho, S.C. Zou and B. Wang, J. Hazard. Mater. 2011, **195**, 346–354.
53 Z.H. Ai, W.K. Ho, S.C. Lee and L.Z. Zhang, Environ. Sci. Technol. 2009, **43**, 4143–4150.
54 J.Y. Xiong, Z.B. Jiao, G.X. Lu, W. Ren, J.H. Ye and Y.P. Bi, Chem. Eur. J. 2013, **19**, 9472–9475.
55 F. Dong, T. Xiong, R. Wang, Y.J. Sun and Y.K. Jiang, Dalton Trans. 2014, **43**, 6631–6642.
56 F. Dong, Q.Y. Li, Y. Zhou, Y.J. Sun, H.D. Zhang and Z.B. Wu, Dalton Trans. 2014, **43**, 9468–9480.
57 W.D. Zhang, Q. Zhang and F. Dong, Ind. Eng. Chem. Res. 2013, **52**, 6740−6746.
58 F. Dong, Z.W. Zhao, T. Xiong, Z.L. Ni, W.D. Zhang, Y.J. Sun and W.K. Ho, ACS Appl. Mater. Interfaces, 2013, **5**, 11392−11401.
59 S.J. Peng, P.N. Zhu, S.G. Mhaisalkar and S. Ramakrishna, J. Phys. Chem. C, 2012, **116**, 13849–13857.
60 M.R. Khan, T.W. Chuan, A. Yousuf, M.N.K. Chowdhury, C.K. Cheng, Catalysis Science & Technology, 2015, **5**, 2522–2531.
61 F. Dong, Q.Y. Li, Y.J. Sun and W.K. Ho, ACS Catal. 2014, **4**, 4341–4350.

Text: The highly visible light active 3D Au/$Bi_2O_2CO_3$ heterostructure was fabricated by a one-pot in situ hydrothermal method.

Color artwork